

Image compression by rectangular wavelet transform

Vyacheslav Zavadsky^a

^a*Semiconductor Insights, R&D department, 3000 Solandt Road, Kanata, ON, Canada. K2K2X2*

Abstract

We study image compression by a separable wavelet basis $\{\psi(2^{k_1}x - i)\psi(2^{k_2}y - j), \phi(x - i)\psi(2^{k_2}y - j), \psi(2^{k_1}(x - i)\phi(y - j), \phi(x - i)\phi(y - i)\}$, where $k_1, k_2 \in \mathbb{Z}_+$; $i, j \in \mathbb{Z}$; and ϕ, ψ are elements of a standard biorthogonal wavelet basis in $L_2(\mathbb{R})$. Because $k_1 \neq k_2$, the supports of the basis elements are rectangles, and the corresponding transform is known as the *rectangular wavelet transform*. We prove that if one-dimensional wavelet basis has M dual vanishing moments then the rate of approximation by N coefficients of rectangular wavelet transform is $\mathcal{O}(N^{-M} \log^C N)$ for functions with mixed derivative of order M in each direction.

The square wavelet transform yields the approximation rate is $\mathcal{O}(N^{-M/2})$ for functions with all derivatives of the total order M . Thus, the rectangular wavelet transform can outperform the square one if an image has a mixed derivative. We provide experimental comparison of image compression which shows that rectangular wavelet transform outperform the square one.

Key words: Non-linear wavelet compression, rectangular wavelet transform, hyperbolic wavelets, anisotropic Besov space, sparse grid.

1 Introduction

Wavelet analysis has become a powerful tool for image and signal processing. Initially developed for approximations and analysis of functions of a single real variable, wavelet techniques was almost immediately generalized for the case of two and many variables.

We will start our discussion with the most recent generalization, *non-separable wavelets*. In this construction, lattice of integers in one dimensional case is

Email address: vyacheslavz@semiconductor.com (Vyacheslav Zavadsky).

replaced by the quincunx or a general lattice in the multi-dimensional case, and a wavelet analysis is derived directly for this lattice (see [?, ?]).

Although the non-separable approach now attracts the majority of researchers, we will focus this paper on comparison of the *square* and the *rectangular* separable wavelets for the two-dimensional case. We will show that the rectangular wavelet transform in some applications is more suitable than classical square one. The “rectangularization” technique can also be applicable to some non-separable wavelet constructions.

Separable approaches involve building a basis in $L_2(\mathbb{R}^d)$ using elements of a wavelet basis for $L_2(\mathbb{R})$. DeVore *et al.* in [?] and numerous other researchers studied the following basis in $L_2(\mathbb{R}^2)$:

$$\left\{ \phi(2^l x - i)\phi(2^l y - j), \psi(2^k x - i)\psi(2^k y - j), \right. \\ \left. \phi(2^k x - i)\psi(2^k y - j), \psi(2^k x - i)\phi(2^k y - j) \right\}, \quad (1)$$

where ϕ is a *scaling function*, ψ is the corresponding wavelet, $l \in \mathbb{Z}$, $k \geq l$, $k \in \mathbb{Z}$, and $i, j \in \mathbb{Z}$.

Because the supports of the basis functions are localized in the squares with sizes $\mathcal{O}(2^{-k} \times 2^{-k})$, the decomposition on this basis is called the *square wavelet transform*. It is well known that if a function has bounded (in a certain space) derivatives of the total order M and $\tilde{\psi}$ has M vanishing moments then the rate of approximation by N elements of this basis is $\mathcal{O}(N^{-M/2})$.

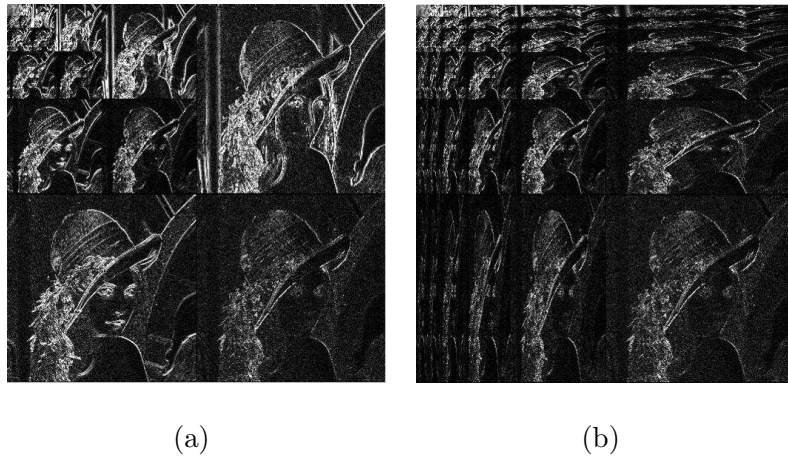


Fig. 1. The Lena images decomposed by square and rectangular wavelet transforms based on the Haar basis.

Rectangular wavelet transform is inspired by approximation theory technique known as “sparse grid”, or “hyperbolic cross” (see, for example, [?]). The square wavelet transform (and its higher dimensional analogs) suffers from so

called “curse of dimensionality”. In order to get the same precision of approximation as by N coefficients in the one dimensional case, one needs to utilize $\mathcal{O}(N^d)$ coefficients for the function of d variables. The “sparse grid” technique allows to build a basis for functions of many variables that yields the same rate of convergence (up to a logarithmic factor) as in the case of one variable. In application to the construction of a wavelet basis, it yields a basis

$$\left\{ \psi(2^{k_1}x - i)\psi(2^{k_2}y - j), \phi(2^l x - i)\psi(2^{k_2}y - j), \right. \\ \left. \psi(2^{k_1}(x - i)\phi(2^l y - j), \phi(x - i)\phi(y - i)) \right\}, \quad (2)$$

where $k_1, k_2 \geq l$, $k_1, k_2 \in \mathbb{Z}$, $i, j \in \mathbb{Z}$ and l is a fixed integer number. Because elements of the basis are supported on rectangles of size $\mathcal{O}(2^{-k_1} \times 2^{-k_2})$, and $k_1 \neq k_2$, the corresponding transform can be called *rectangular*.

The application of this basis to the problem of multivariate surface denoising was studied in [?] and [?]. The approximation properties of the rectangular wavelet transform in Besov spaces was studied DeVore *et al.* in [?], and by Zavadsky in [?].

This paper aims at providing a self contained study of the approximation properties of the rectangular wavelet transform from the perspective of image processing and benchmarking of the rectangular transforms with respect to the square one for image compression.

We show that if the approximated function has the mixed derivative of total order $2M$ and $\tilde{\psi}$ has M vanishing moments, then the rate of approximation by N elements of this basis is $\mathcal{O}(N^{-M} \log^C N)$.

The rest of the paper is organized as follows. In section 2, we recall some basic properties of one dimensional wavelet bases. In section 3, we consider our motivations for migration from square wavelet transform to rectangular one. In section 4, we consider approximation rates of the non-linear approximations by the rectangular wavelet basis in $L_p(\mathbb{R}^2)$, $1 \leq p < \infty$. In section 5, we provide numerical experiments results on standard test images.

2 One-dimensional wavelet transform

Biorthogonal bases of compactly supported wavelets were build in [?]. Following this paper, we assume that we have four compactly supported functions $\phi, \tilde{\phi}, \psi, \tilde{\psi} \in L_\infty(\mathbb{R})$ and coefficients vectors $h, \tilde{h}, g, \tilde{g}$ that satisfy the following

conditions:

$$\phi(x) = \sum_{i \in \mathbb{Z}} h_i \phi(2x - i), \quad (3)$$

$$\tilde{\phi}(x) = \sum_{i \in \mathbb{Z}} \tilde{h}_i \tilde{\phi}(2x - i), \quad (4)$$

$$\psi(x) = \sum_{i \in \mathbb{Z}} g_i \phi(2x - i), \quad (5)$$

$$\tilde{\psi}(x) = \sum_{i \in \mathbb{Z}} \tilde{g}_i \tilde{\phi}(2x - i), \quad (6)$$

$$\langle \phi(x), \tilde{\phi}(x - i) \rangle = \begin{cases} 1 \text{ if } i = 0, \\ 0 \text{ otherwise,} \end{cases} \quad i \in \mathbb{Z}, \quad (7)$$

$$\langle \psi, \tilde{\psi}(2^k x - i) \rangle = \begin{cases} 1 \text{ if } i = 0 \text{ and } k = 0, \\ 0 \text{ otherwise,} \end{cases} \quad i, k \in \mathbb{Z}, \quad (8)$$

$$\langle \phi, \tilde{\psi}(2^k x - i) \rangle = \begin{cases} 1 \text{ if } i = 0 \text{ and } k = 0, \\ 0 \text{ otherwise,} \end{cases} \quad i \in \mathbb{Z}, k \in \mathbb{Z}_+, \quad (9)$$

$$\langle \psi, \tilde{\phi}(2^k x - i) \rangle = \begin{cases} 1 \text{ if } i = 0 \text{ and } k = 0, \\ 0 \text{ otherwise,} \end{cases} \quad i \in \mathbb{Z}, k \in \mathbb{Z}_-, \quad (10)$$

where $\langle f_1(x), f_2(x) \rangle = \int f_1(x) f_2(x) dx$. We further assume that the basis has M dual vanishing moments:

$$\int x^k \tilde{\psi}(x) dx = 0, \quad k = 0, \dots, M-1. \quad (11)$$

It can be shown that for any scale $l \in \mathbb{Z}$ any function $f \in L_2(\mathbb{R})$ can be represented as

$$f(x) = \sum_{i \in \mathbb{Z}} 2^l \phi(2^l x - i) \alpha_{l,i} + \sum_{k=l}^{\infty} 2^k \psi(2^k x - i) \beta_{k,i}, \quad (12)$$

$$\text{where } \alpha_{k,i} = \langle f, \tilde{\phi}(2^k x - i) \rangle, \quad (13)$$

$$\beta_{k,i} = \langle f, \tilde{\psi}(2^k x - i) \rangle. \quad (14)$$

The *fast wavelet transform* allows to quickly go in representation (12) from scale l to $l-1$ and back (*inverse fast wavelet transform*) by observing that

$$\alpha_{l-1,i} = \langle f, \tilde{\phi}(2^{l-1} x - i) \rangle = \sum_{j \in \mathbb{Z}} \tilde{h}_j \langle f, \tilde{\phi}(2^l x - 2i - j) \rangle = \sum_{j \in \mathbb{Z}} \tilde{h}_j \alpha_{l,2i+j}, \quad (15)$$

$$\beta_{l-1,i} = \langle f, \tilde{\psi}(2^{l-1} x - i) \rangle = \sum_{j \in \mathbb{Z}} \tilde{g}_j \langle f, \tilde{\phi}(2^l x - 2i - j) \rangle = \sum_{j \in \mathbb{Z}} \tilde{g}_j \alpha_{l,2i+j}, \quad (16)$$

$$\begin{aligned}
\alpha_{l,i} = & \langle f, \tilde{\phi}(2^l x - i) \rangle = 2^{l-1} \sum_{j \in \mathbb{Z}} \alpha_{l-1,j} \langle \phi(2^{l-1} x - j), \tilde{\phi}(2^l x - i) \rangle + \\
& + 2^{l-1} \sum_{j \in \mathbb{Z}} \beta_{l-1,j} \langle \psi(2^{l-1} x - j), \tilde{\phi}(2^l x - i) \rangle + \\
& + \sum_{k=l}^{\infty} 2^{k-1} \sum_{j \in \mathbb{Z}} \beta_{k-1,j} \langle \psi(2^k x - j), \tilde{\phi}(2^l x - i) \rangle. \quad (17)
\end{aligned}$$

According to (10) the last term is 0. Expanding $\phi(2^{l-1}x - j)$ and $\psi(2^{l-1}x - j)$ by (3) and (5) and then using (7), one can show that

$$\alpha_{l,i} = \frac{1}{2} \left[\sum_{j \in \mathbb{Z}} h_{2j-i} \alpha_{l-1,j} + \sum_{j \in \mathbb{Z}} g_{2j-i} \beta_{l-1,j} \right] \quad (18)$$

In practice, if we process a discrete signal sampled with step 2^{-l} , it is typically assumed that in expansion (12) $\beta_{k,i} = 0$ and $\alpha_{l,i}$ are the discrete values of observed signal.

The wavelet transform is typically used to compress or denoise signals by moving to representation (12) with smaller l by iterative applications of (15),(16); setting certain $\beta_{k,i}$ to 0 (that will reduce data size and filter out random noise); and moving back to the original l by iterative application of (18).

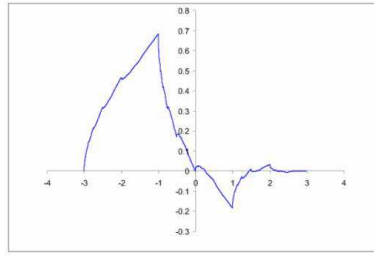
3 Motivation

Let us start from considering square wavelet transform build from the D4 Daubechies orthogonal wavelet with 2 vanishing moments, see Fig. 2. As we see, the $\phi(x)\psi(y)$ term characterizes horizontal edges, $\psi(x)\phi(y)$ —vertical edges. Although some authors suggested that $\psi(x)\psi(y)$ can be used to characterize edges in the diagonal directions, we can see that this term have different structure from the previous two and we can expect that the corresponding coefficients will decline with different speed.

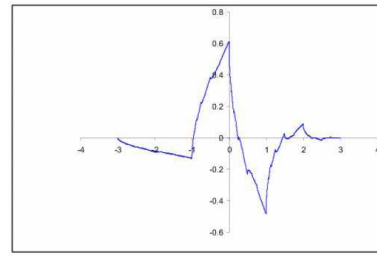
Now let us have a look at Figs. 1(a), 3(a), and 3(c). We can see that the diagonal squares, that are shows coefficients of $\psi(2^k x - i)\psi(2^k y - j)$ are less bright than others.

Now let us consider how the value of coefficients with terms $\psi(x)\psi(y)$ and $\phi(x)\psi(y)$, $\psi(x)\phi(y)$ can be compared from the theoretical standpoint. The proof of the following lemma is given in Appendix:

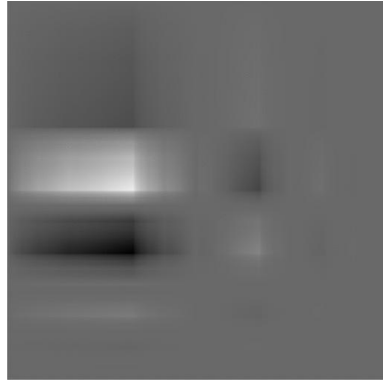
Lemma 1 *For any wavelet basis with M dual vanishing moments and for any $p \geq 1$ there exist constants C, L such that for any $\sigma_1, \sigma_2 > 0$ and $\theta_1, \theta_2 \in \mathbb{R}$*



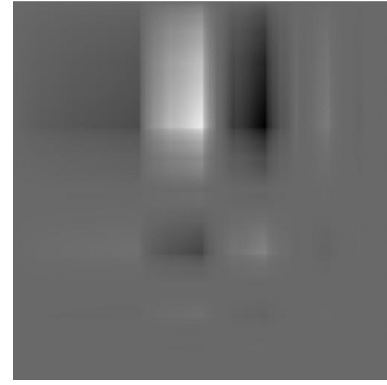
(a) Scaling function $\phi = \tilde{\phi}$



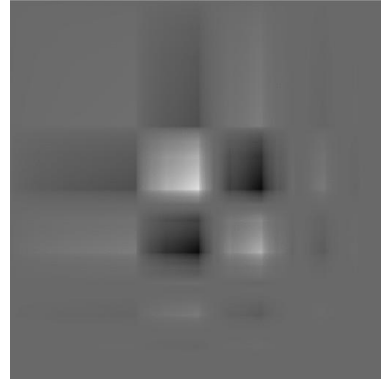
(b) Wavelet function $\psi = \tilde{\psi}$



(c) $\phi(x)\psi(y)$



(d) $\psi(x)\phi(y)$

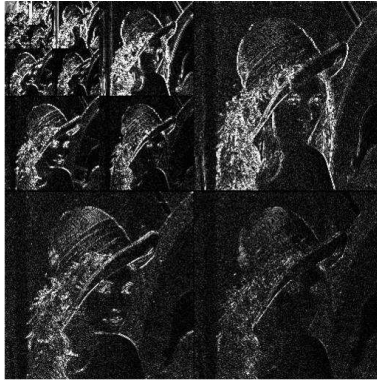


(e) $\psi(x)\psi(y)$

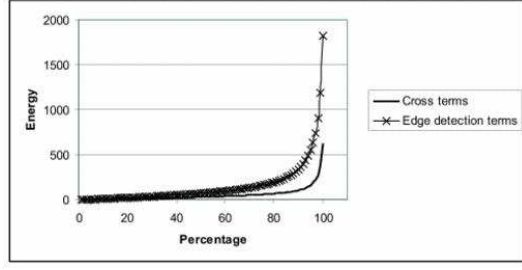
Fig. 2. D4: the Daubechies orthogonal wavelet with 2 vanishing moments and elements of square wavelet basis built from it.

and for any function $f(x, y)$ with the appropriate derivative in L_p^{loc} :

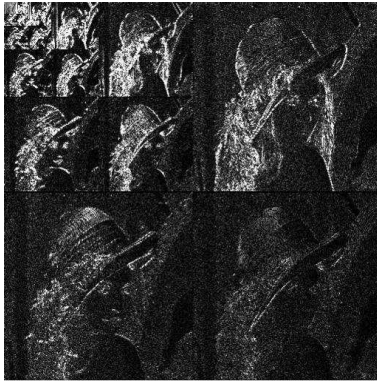
$$\begin{aligned} & \left| \langle f(x, y), \tilde{\psi}(\sigma_1 x - \theta_1) \tilde{\phi}(\sigma_2 y - \theta_2) \rangle \right| \leq \\ & \leq C \frac{1}{\sigma_1^{M+1-1/p}} \left[\int_{\frac{\theta_1-L}{\sigma_1}}^{\frac{\theta_1+L}{\sigma_1}} \int_{\frac{\theta_2-L}{\sigma_2}}^{\frac{\theta_2+L}{\sigma_2}} \left| \frac{d^M}{dx^M} f(x, y) \right|^p dy dx \right]^{1/p}, \quad (19) \end{aligned}$$



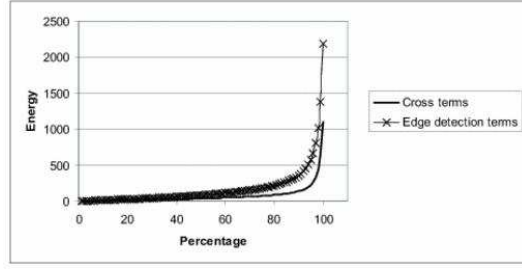
(a) D4 decomposition



(b) D4 energy distribution



(c) CRF(13,7) decomposition



(d) CRF(13,7) energy distribution

Fig. 3. The Lena image decomposed by square wavelet transform built from the Daubechies orthogonal D4 filter and the JPEG2000 CRF(13,7) filter. The energy distribution plots in (b), (d) show the distribution of L_2 norms of $\beta\phi(x)\psi(y)$, $\beta\psi(x)\phi(y)$ (edge detection terms) and $\beta\psi(x)\psi(y)$ (cross terms).

$$\left| \langle f(x, y), \tilde{\phi}(\sigma_1 x - \theta_1) \tilde{\psi}(\sigma_2 y - \theta_2) \rangle \right| \leq C \frac{1}{\sigma_2^{M+1-1/p}} \left[\int_{\frac{\theta_1-L}{\sigma_1}}^{\frac{\theta_1+L}{\sigma_1}} \int_{\frac{\theta_2-L}{\sigma_2}}^{\frac{\theta_2+L}{\sigma_2}} \left| \frac{d^M}{dy^M} f(x, y) \right|^p dy dx \right]^{1/p}, \quad (20)$$

$$\left| \langle f(x, y), \tilde{\psi}(\sigma_1 x - \theta_1) \tilde{\psi}(\sigma_2 y - \theta_2) \rangle \right| \leq C \frac{1}{(\sigma_1 \sigma_2)^{M+1-1/p}} \left[\int_{\frac{\theta_1-L}{\sigma_1}}^{\frac{\theta_1+L}{\sigma_1}} \int_{\frac{\theta_2-L}{\sigma_2}}^{\frac{\theta_2+L}{\sigma_2}} \left| \frac{d^{2M}}{dx^M dy^M} f(x, y) \right|^p dy dx \right]^{1/p}. \quad (21)$$

4 Non-linear approximation

Theorem 2 For any wavelet basis with M dual vanishing moments and for any $p \geq \max(1, 1/M)$; $q \geq 1$ there exists a constant C such that any function $f(x, y)$ with support localized in $[0, 1]^2$ and the mixed derivative $\frac{d^{2M}}{dx^M dy^M} f(x, y) \in L_p$ for any $N > 0$ can be approximated by a function f_N such that

$$\|f - f_N\|_{L_q} \leq CN^{-M} \left\| \frac{d^{2M}}{dx^M dy^M} f(x, y) \right\|_{L_p} \log^C N, \quad (22)$$

where f_N has non more than CN non zero coefficients in the expansion on the rectangular wavelet basis.

PROOF. Denote:

$$\mathcal{I} = \mathbb{Z}^2, \quad (23)$$

$$\mathcal{L} = \mathbb{Z}_+^2, \quad (24)$$

$$\phi_{\mathbf{i}} = \phi(x - i_1)\phi(x - i_2), \quad (i_1, i_2) \in \mathcal{I}, \quad (25)$$

$$\tilde{\phi}_{\mathbf{i}} = \tilde{\phi}(x - i_1)\tilde{\phi}(x - i_2), \quad (26)$$

$$\psi_{\mathbf{l}, \mathbf{i}} = \psi(2^{l_1}x - i_1)\psi(2^{l_2}y - i_2), \quad (l_1, l_2) \in \mathcal{L}, (i_1, i_2) \in \mathcal{I}, \quad (27)$$

$$\tilde{\psi}_{\mathbf{l}, \mathbf{i}} = \tilde{\psi}(2^{l_1}x - i_1)\tilde{\psi}(2^{l_2}y - i_2), \quad (28)$$

$$\alpha_{\mathbf{i}} = \langle f, \tilde{\phi}_{\mathbf{i}} \rangle, \quad (29)$$

$$\beta_{\mathbf{l}, \mathbf{i}} = \langle f, \tilde{\psi}_{\mathbf{l}, \mathbf{i}} \rangle, \quad (30)$$

$$\|\mathbf{l}\| = l_1 + l_2, \quad (l_1, l_2) \in \mathcal{L}, \quad (31)$$

$$\mathcal{D} = \left\| \frac{d^{2M}}{dx^M dy^M} f(x, y) \right\|_{L_p}. \quad (32)$$

Because the set $\{\phi_{\mathbf{i}}, \psi_{\mathbf{l}, \mathbf{i}} \mid \mathbf{i} \in \mathcal{I}, \mathbf{l} \in \mathcal{L}\}$ is the tensor product of the wavelet basis in $L_q(\mathbb{R})$, it forms a basis in $L_q(\mathbb{R}^2)$ and

$$f(x, y) = \sum_{\mathbf{i} \in \mathcal{I}} \alpha_{\mathbf{i}} \phi_{\mathbf{i}} + \sum_{\mathbf{l} \in \mathcal{L}} 2^{\|\mathbf{l}\|} \sum_{\mathbf{i} \in \mathcal{I}} \beta_{\mathbf{l}, \mathbf{i}} \psi_{\mathbf{l}, \mathbf{i}}. \quad (33)$$

Because $f(x, y)$ is compactly supported, there exists a constant C such that for any $\mathbf{l} \in \mathcal{L}$

$$\mathcal{N}(\|\mathbf{l}\|) = \left| \left\{ \mathbf{i} \mid \mathbf{i} \in \mathcal{I}, \beta_{\mathbf{l}, \mathbf{i}} \neq 0 \right\} \right| \leq C 2^{\|\mathbf{l}\|} + C, \quad (34)$$

where here and below C denotes the universal constant that is maximum of all appropriate constants in the proof and depends only on the wavelet basis, p , and q .

Denote by l_0 the maximum l such that $l^2\mathcal{N}(l) \leq N$.

Define

$$\epsilon_l = \mathcal{D}/2^{l+\frac{M+1/p}{2}l_0+\frac{M-1/p}{2}l}. \quad (35)$$

Let

$$f_N = \sum_{\mathbf{i} \in \mathcal{I}} \alpha_{\mathbf{i}} \phi_{\mathbf{i}} + \sum_{\mathbf{l} \in \mathcal{L}} 2^{\|\mathbf{l}\|} \sum_{\mathbf{i} \in \mathcal{I}} \tilde{\beta}_{\mathbf{l}, \mathbf{i}} \psi_{\mathbf{l}, \mathbf{i}}, \quad (36)$$

where

$$\tilde{\beta}_{\mathbf{l}, \mathbf{i}} = \begin{cases} 0, & \text{if } \|\mathbf{l}\| > l_0 \text{ and } \beta_{\mathbf{l}, \mathbf{i}} \leq \epsilon_{\|\mathbf{l}\|}, \\ \beta_{\mathbf{l}, \mathbf{i}} & \text{otherwise.} \end{cases} \quad (37)$$

Now let us calculate the number of non-zero coefficients \tilde{N} in $\tilde{\beta}_{\mathbf{l}, \mathbf{i}}$. From (21) it follows that for any fixed \mathbf{l}

$$\|\beta_{\mathbf{l}, \cdot}\|_{l_p} \leq C\mathcal{D}/2^{\|\mathbf{l}\|(M+1-1/p)}. \quad (38)$$

Let us note that if $\|\beta\|_{l_p} < A$ then the number of coefficients bigger than $\epsilon > 0$ in β can not exceed A^p/ϵ^p . Taking into account (34), we have

$$\tilde{N} \leq C \sum_{l=0}^{l_0} l(2^l + C) + \sum_{l=l_0+1}^{\infty} l \frac{\mathcal{D}^p}{2^{lp(M+1-1/p)} \epsilon_l^p} \leq CN. \quad (39)$$

Because $\psi \in L_{\infty}$ and is compactly supported,

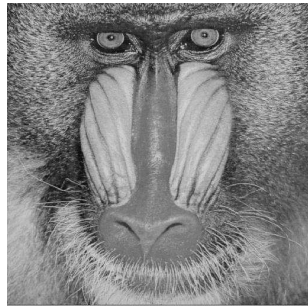
$$\begin{aligned} \|f - f_N\|_{L_q} &\leq C \sum_{l=l_0+1}^{\infty} l 2^l \epsilon_l = \\ &= C\mathcal{D} \sum_{l=l_0+1}^{\infty} l / 2^{\frac{M+1/p}{2}l_0 + \frac{M-1/p}{2}l} \leq CN^{-M} \left\| \frac{d^{2M}}{dx^M dy^M} f(x, y) \right\|_{L_p} \log^C N \end{aligned} \quad (40)$$

□

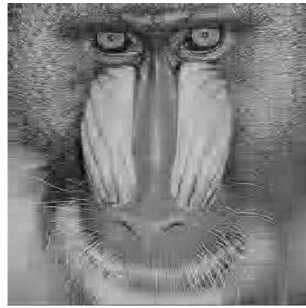
5 Experiments

To numerically compare results of square and rectangular wavelet transform we limited ourselves to the problem of image compression. We took the standard 512×512 “Mandrill”, “House”, “Lena”, and “Barbara” greyscale images and compress them to reduce the number of non-zero coefficients by factors of 80 and 160¹. The results are shown in Figs 4, 5, 6, and 7.

¹ Some papers on image compression use 256×256 images. For the same quality, they report 4 times smaller compression numbers.



(a) The original "Mandrill" 512×512 image.



(b) D4 orthogonal wavelet, compression 1:83, rectangular transform.



(c) D4 orthogonal wavelet, compression 1:83, square transform.



(d) CRF(13,7) biorthogonal wavelet, compression 1:87, rectangular transform.



(e) CRF(13,7) biorthogonal wavelet, compression 1:81, square transform.



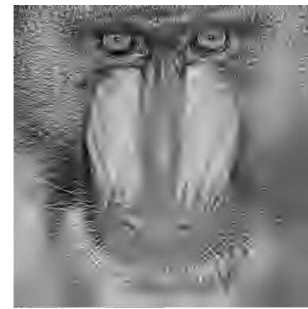
(f) D4 orthogonal wavelet, compression 1:172, rectangular transform.



(g) D4 orthogonal wavelet, compression 1:167, square transform.



(h) CRF(13,7) biorthogonal wavelet, compression 1:163, rectangular transform.



(i) CRF(13,7) biorthogonal wavelet, compression 1:166, square transform.

Fig. 4. The Mandrill image compressed by the rectangular and square wavelet transforms.



(a) The original "House" 512×512 image.



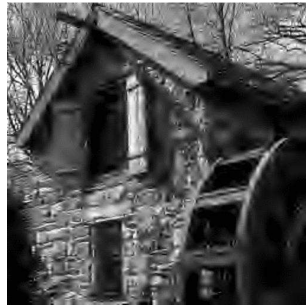
(b) D4 orthogonal wavelet, compression 1:89, rectangular transform.



(c) D4 orthogonal wavelet, compression 1:86, square transform.



(d) CRF(13,7) biorthogonal wavelet, compression 1:82, rectangular transform.



(e) CRF(13,7) biorthogonal wavelet, compression 1:79, square transform.



(f) D4 orthogonal wavelet, compression 1:163, rectangular transform.



(g) D4 orthogonal wavelet, compression 1:166, square transform.



(h) CRF(13,7) biorthogonal wavelet, compression 1:163, rectangular transform.



(i) CRF(13,7) biorthogonal wavelet, compression 1:162, square transform.

Fig. 5. The "House" image compressed by the rectangular and square wavelet transforms.



(a) The original "Lena" 512×512 image.



(b) D4 orthogonal wavelet, compression 1:87, rectangular transform.



(c) D4 orthogonal wavelet, compression 1:86, square transform.



(d) CRF(13,7) biorthogonal wavelet, compression 1:85, rectangular transform.



(e) CRF(13,7) biorthogonal wavelet, compression 1:84, square transform.



(f) D4 orthogonal wavelet, compression 1:160, rectangular transform.



(g) D4 orthogonal wavelet, compression 1:166, square transform.



(h) CRF(13,7) biorthogonal wavelet, compression 1:162, square transform.



(i) CRF(13,7) biorthogonal wavelet, compression 1:163, square transform.

Fig. 6. The "Lena" image compressed by the rectangular and square wavelet transforms.



(a) The original "Barbara" 512×512 image.



(b) D4 orthogonal wavelet, compression 1:80, rectangular transform.



(c) D4 orthogonal wavelet, compression 1:92, square transform.



(d) CRF(13,7) biorthogonal wavelet, compression 1:88, rectangular transform.



(e) CRF(13,7) biorthogonal wavelet, compression 1:83, square transform.



(f) D4 orthogonal wavelet, compression 1:166, square transform.



(g) D4 orthogonal wavelet, compression 1:169, square transform.



(h) CRF(13,7) biorthogonal wavelet, compression 1:166, rectangular transform.



(i) CRF(13,7) biorthogonal wavelet, compression 1:164, square transform.

Fig. 7. The "Barbara" image compressed by the rectangular and square wavelet transforms.

We believe that results clearly show that the rectangular wavelet transform visually outperforms the square one for all test images. Although the effect is more visible on the Mandrill and Barbara images and less visible on the Lena and House images, in all cases, the results of rectangular compression at the 1:160 rate are visually close to the results of square compression at the 1:80 rate.

6 Conclusions

As we shown, the rectangular wavelet transform has substantially better convergence rate if the approximated function has the mixed derivative of appropriate order. In this case, it allows to solve the "curse of dimensionality" issue and gives the same degree of approximation (up to a logarithmic factor) as the wavelet basis in the one dimensional case.

From the results of numerical experiments we can see that the mixed derivative assumption is reasonable for the standard test images and rectangular wavelet transform allows to improve the compression rate (measured in the number of non-zero coefficient) by factor of 2.

It would be worthwhile to investigate what actual bit rate compression an industrial grade image compression algorithm (such as JPEG2000) will produce if the square wavelet transform is replaced by rectangular one.

Although further experiments in this direction are needed, we believe that it's worthwhile to investigate the applicability of rectangular wavelet transform to video compression. Because the actual dimension of data in this case is 3, the solution to the "curse of dimensionality" can be particularly beneficial in this case. Although certain technical work to organize codec to ensure intermediate frame recovery is needed, the results can be quite interesting not only from the actual bit-rate standpoint, but also because expensive movement search operation is replaced by a straightforward fast wavelet decomposition.

The rectangular wavelet transform is especially efficient to represent details that are either in the horizontal or vertical directions. Certain second generation schemes (such as wavelets for the quincunx lattice) can be modified in to ensure the same rate of convergence for the functions with bounded mixed derivative as in the case of the rectangular wavelet transform. This may further improve the results.

7 Appendix: proof of Lemma 1

Because we assumed that $\tilde{\psi}$ is compactly supported, there exists $L > 0$ such that $|x| \geq L \Rightarrow \tilde{\psi}(x) = 0$. Let us define functions $\tilde{\Psi}_m$ for $m \in \mathbb{N}$ as follows:

$$\tilde{\Psi}_m(x) := \int_{-L}^x \tau^{m-1} \tilde{\psi}(\tau) d\tau. \quad (41)$$

Because $\tilde{\psi} \in L_\infty$, $\tilde{\Psi}_m(x) \in L_\infty^{loc}$. Moreover, because $\tilde{\psi}$ has M vanishing moments $\tilde{\Psi}_m$ is supported on $[-L, L]$ for $m \leq M$.

Lemma 1 is a combination of the following results:

Lemma 3 *For any function $f(x)$ with M -th derivative*

$$\langle f(x), \tilde{\psi}(\sigma x - \theta) \rangle = \frac{1}{\sigma^M} \int_{\frac{\theta-L}{\sigma}}^{\frac{\theta+L}{\sigma}} f^{(M)}(x) \tilde{\Psi}_M(\sigma x - \theta) dx. \quad (42)$$

PROOF.

$$\begin{aligned} \langle f(x), \tilde{\psi}(\sigma x - \theta) \rangle &= \int_{\frac{\theta-L}{\sigma}}^{\frac{\theta+L}{\sigma}} f(x) \tilde{\psi}(\sigma x - \theta) dx = \\ &= \int_{\frac{\theta-L}{\sigma}}^{\frac{\theta+L}{\sigma}} f'(x) \int_{\frac{\theta-L}{\sigma}}^x \tilde{\psi}(\sigma \tau - \theta) d\tau dx = \dots = \\ &= \int_{\frac{\theta-L}{\sigma}}^{\frac{\theta+L}{\sigma}} f^{(M)}(x) \int_{\frac{\theta-L}{\sigma}}^x \left[\tau - \frac{\theta-L}{\sigma} \right]^{M-1} \tilde{\psi}(\sigma \tau - \theta) d\tau dx. \end{aligned} \quad (43)$$

Lemma 4 *For any wavelet basis with M dual vanishing moments and for any $p \geq 1$ there exist constants C, L such that for any $\sigma > 0$ and $\theta \in \mathbb{R}$ and for any function f with M -th derivative in L_p^{loc}*

$$\left| \langle f(x), \tilde{\psi}(\sigma x - \theta) \rangle \right| \leq C \frac{1}{\sigma^{M+1-1/p}} \left[\int_{\frac{\theta-L}{\sigma}}^{\frac{\theta+L}{\sigma}} |f^{(M)}(x)|^p dx \right]^{1/p}. \quad (44)$$

Moreover, if the basis does not has $M+1$ dual vanishing moments, then there exists a function f such that

$$\left| \langle f(x), \tilde{\psi}(\sigma x - \theta) \rangle \right| \geq \frac{1}{C} \frac{1}{\sigma^{M+1-1/p}} \left[\int_{\frac{\theta-L}{\sigma}}^{\frac{\theta+L}{\sigma}} |f^{(M)}(x)|^p dx \right]^{1/p}. \quad (45)$$

PROOF. Denote $\mathcal{N}_q := \|\tilde{\Psi}_M\|_{L_q}$. Let us note that $\mathcal{N}_q < \infty$ for $q > 0$.

By applying the Hölder inequality to (42), we get

$$\left| \langle f(x), \tilde{\psi}(\sigma x - \theta) \rangle \right| \leq \frac{\mathcal{N}_{1/(1-1/p)}}{\sigma^{M+1-1/p}} \left[\int_{\frac{\theta-L}{\sigma}}^{\frac{\theta+L}{\sigma}} |f^{(M)}(x)|^p dx \right]^{1/p}. \quad (46)$$

To proof (45), consider $f(x) = x^M/M!$. After substituting it to (42):

$$\left\langle \frac{x^M}{M!}, \tilde{\psi}(\sigma x - \theta) \right\rangle = \frac{1}{\sigma^{M+1}} \tilde{\Psi}_{M+1}(L). \quad (47)$$

Note that since $\tilde{\psi}$ does not has $M+1$ vanishing moments, $\tilde{\Psi}_{M+1}(L) \neq 0$. Taking into the account that

$$\left[\int_{\frac{\theta-L}{\sigma}}^{\frac{\theta+L}{\sigma}} 1 dx \right]^{1/p} = (2L/\sigma)^{1/p}, \quad (48)$$

and putting $C = \max((2L)^{1/p}/|\tilde{\Psi}_{M+1}(L)|, \mathcal{N}_{1/(1-1/p)})$, we conclude the proof.

Corollary 5 *For any wavelet basis with M dual vanishing moments and for any $p \geq 1$ there exist constants C, L such that for any $\sigma_1, \sigma_2 > 0$ and $\theta_1, \theta_2 \in \mathbb{R}$ and for any function $f(x, y)$ with the appropriate derivative in L_p^{loc} :*

$$\begin{aligned} \left| \langle f(x, y), \tilde{\psi}(\sigma_1 x - \theta_1) \tilde{\phi}(\sigma_2 y - \theta_2) \rangle \right| &\leq \\ &\leq C \frac{1}{\sigma_1^{M+1-1/p}} \left[\int_{\frac{\theta_1-L}{\sigma_1}}^{\frac{\theta_1+L}{\sigma_1}} \int_{\frac{\theta_2-L}{\sigma_2}}^{\frac{\theta_2+L}{\sigma_2}} \left| \frac{d^M}{dx^M} f(x, y) \right|^p dy dx \right]^{1/p}, \end{aligned} \quad (49)$$

$$\begin{aligned} \left| \langle f(x, y), \tilde{\phi}(\sigma_1 x - \theta_1) \tilde{\psi}(\sigma_2 y - \theta_2) \rangle \right| &\leq \\ &\leq C \frac{1}{\sigma_2^{M+1-1/p}} \left[\int_{\frac{\theta_1-L}{\sigma_1}}^{\frac{\theta_1+L}{\sigma_1}} \int_{\frac{\theta_2-L}{\sigma_2}}^{\frac{\theta_2+L}{\sigma_2}} \left| \frac{d^M}{dy^M} f(x, y) \right|^p dy dx \right]^{1/p}. \end{aligned} \quad (50)$$

Lemma 6 *For any wavelet basis with M dual vanishing moments and for any $p \geq 1$ there exist constants C, L such that for any $\sigma_1, \sigma_2 > 0$ and $\theta_1, \theta_2 \in \mathbb{R}$ and for any function $\frac{d^{2M}}{dx^M dy^M} f(x, y) \in L_p^{loc}$:*

$$\begin{aligned} \left| \langle f(x, y), \tilde{\psi}(\sigma_1 x - \theta_1) \tilde{\psi}(\sigma_2 y - \theta_2) \rangle \right| &\leq \\ &\leq C \frac{1}{(\sigma_1 \sigma_2)^{M+1-1/p}} \left[\int_{\frac{\theta_1-L}{\sigma_1}}^{\frac{\theta_1+L}{\sigma_1}} \int_{\frac{\theta_2-L}{\sigma_2}}^{\frac{\theta_2+L}{\sigma_2}} \left| \frac{d^{2M}}{dx^M dy^M} f(x, y) \right|^p dy dx \right]^{1/p}. \end{aligned} \quad (51)$$

PROOF. Let us consider

$$\begin{aligned} g(y) &= \int f(x, y) \tilde{\psi}(\sigma_1 x - \theta) dx = \\ &= \frac{1}{\sigma_1^M} \int_{\frac{\theta_1-L}{\sigma_1}}^{\frac{\theta_1+L}{\sigma_1}} \frac{d^M}{dx^M} f(x, y) \tilde{\Psi}_M(\sigma_1 x - \theta_1) dx. \end{aligned} \quad (52)$$

Then

$$\begin{aligned} &< f(x, y), \tilde{\psi}(\sigma_1 x - \theta_1) \tilde{\psi}(\sigma_2 y - \theta_2) > = < g(y), \tilde{\psi}(\sigma_2 y - \theta_2) > = \\ &= \frac{1}{\sigma_1^M \sigma_2^M} \int_{\frac{\theta_2-L}{\sigma_2}}^{\frac{\theta_2+L}{\sigma_2}} \tilde{\Psi}_M(\sigma_2 y - \theta_2) \frac{d^M}{dy^M} \int_{\frac{\theta_1-L}{\sigma_1}}^{\frac{\theta_1+L}{\sigma_1}} \frac{d^M}{dx^M} f(x, y) \tilde{\Psi}_M(\sigma_1 x - \theta_1) dx dy \end{aligned} \quad (53)$$

Because $\frac{d^{2M}}{dx^M dy^M} f(x, y)$ and $\tilde{\Psi}_M$ are absolutely integrable, we can differentiate under the integral sign:

$$\begin{aligned} &< f(x, y), \tilde{\psi}(\sigma_1 x - \theta_1) \tilde{\psi}(\sigma_2 y - \theta_2) > = \\ &= \frac{1}{\sigma_1^M \sigma_2^M} \int_{\frac{\theta_1-L}{\sigma_1}}^{\frac{\theta_1+L}{\sigma_1}} \int_{\frac{\theta_2-L}{\sigma_2}}^{\frac{\theta_2+L}{\sigma_2}} \tilde{\Psi}_M(\sigma_1 x - \theta_1) \tilde{\Psi}_M(\sigma_2 y - \theta_2) \frac{d^{2M}}{dx^M dy^M} f(x, y) dy dx \end{aligned} \quad (54)$$

By applying the Hölder inequality we conclude the proof.